FEL OPERATION MODES OF THE MAX IV SHORT PULSE FACILITY

Alan Mak*, Francesca Curbis, Sverker Werin, MAX IV Laboratory, Lund University, Sweden

Abstract

The Short Pulse Facility (SPF) of the MAX IV Laboratory in Lund, Sweden features the production of ultrashort, incoherent x-ray pulses. It is driven by a 3-GeV linac and comprises two 5-metre undulator modules. While the SPF is designed for spontaneous radiation, we explore alternative operation modes in which the SPF functions as a simple free-electron laser (FEL). In this article, we characterize two of them in time-dependent numerical simulations. We perform a sensitivity study on the electron beam parameters and examine the technique of single-step tapering.

INTRODUCTION

The MAX IV facility in Lund, Sweden includes a Short Pulse Facility (SPF) [1] in addition to two storage rings. Commissioning is in progress as of 2015.

The SPF is situated at the end of the 3-GeV injector (see Fig. 1). It consists of two variable-gap, planar undulator modules, with a length of 5 metres each. The injector provides short electron bunches, which enable the SPF to produce incoherent x-ray pulses as short as 100 fs. From the same injector, electrons are also extracted at 1.5 GeV and 3 GeV for the top-up of the two storage rings (see Fig. 1).

In addition, the MAX IV facility was designed to enable future expansion. Two x-ray FELs (shown in grey in Fig. 1) can potentially be constructed as branch lines parallel to the SPF. They are set out in the long-term strategic plan of the laboratory [2]. In one of the branch lines, an extra linac section is envisaged, so as to provide the FEL with an electron energy of 5 – 6 GeV.

While the SPF is designed for spontaneous radiation, we explore alternative operation modes which enable the observation of coherent gain as a result of self-amplified spontaneous emission (SASE). In these operation modes, the SPF functions as a simple FEL, whereby the necessary techniques for a full-fledged FEL can be developed and tested.

To lay the foundation for future experimental work, we investigate two of such operation modes with the simulation code GENESIS [3]. In the first case, we study the sensitivity of the radiation power to the electron beam parameters. In the second case, we study the technique of single-step tapering [4, 5].

THEORETICAL BACKGROUND

Saturation Length and Power

Many properties of a high-gain FEL are characterized by the dimensionless Pierce parameter, which is defined as [6]

$$\rho = \frac{1}{2\gamma}\left(\frac{I}{I_A}\right)^{1/3}\left(\frac{\lambda_w K f_B}{2\sqrt{2}\pi\sigma_x}\right)^{2/3}. \quad (1)$$

Here γ is the electron beam energy normalized to the electron rest energy $m_e c^2$. I is the peak current. $I_A = m_e c^3/e = 17.045$ kA is the Alfvén current. σ_x is the rms radius of the electron beam. λ_w is the undulator period. K is the undulator parameter. $f_B = J_0(\xi) - J_1(\xi)$ is the Bessel factor for planar undulators, with $\xi = K^2/[2(K^2+2)]$.

Using the Pierce parameter, the saturation length can be estimated by the relation

$$L_{\mathrm{sat}} \approx \frac{\lambda_w}{\rho}, \quad (2)$$

and the saturation power by the relation

$$P_{\mathrm{sat}} \approx \rho P_{\mathrm{beam}}, \quad (3)$$

where $P_{\mathrm{beam}} = \gamma m_e c^2 I/e$ is the electron beam power [6]. According to these relations, L_{sat} decreases with ρ, while P_{sat} increases with ρ.

In the SPF, the total undulator length L_w is only 10 m. In order to observe exponential power growth, it is preferable to choose an operation mode with $L_{\mathrm{sat}} < L_w$, so that the exponential growth regime will, in principle, occur completely within the undulator line.

Single-Step Tapering

The purpose of single-step tapering is to enhance the power, and hence the energy extraction efficiency, of an FEL. It involves the use of two undulator segments with different undulator parameters. While the parameter of the first segment is K, the parameter of the second segment is decreased to $K - \Delta K$. A recent work by Li and Jia [5] provides a theoretical estimate of the optimal ΔK, given by

$$\frac{\Delta K}{K} = 2\sqrt{2}\rho\left(1 + \frac{2}{K^2}\right). \quad (4)$$

According to this relation, the optimal ΔK depends on the Pierce parameter ρ.

OPERATION MODES

We study two selected operation modes of the SPF using the simulation code GENESIS [3] in the time-dependent mode. The main parameters are shown in Table 1.

In Table 1, the saturation length L_{sat} and saturation power P_{sat} are estimated by Eqs. (2) and (3). For case A, the parameters are chosen so that the estimated L_{sat} is slightly shorter than the total undulator length L_w. For case B, the parameters are chosen so that the estimated L_{sat} is within the first of the two undulator modules.

In the simulations, there is a break section of 1 m between the two 5-metre-long undulator modules. As in the real facility, no focusing elements are inserted to the break section. The electron beam size in the SPF can be adjusted only by changing the twiss parameters at the entrance.

* alan.mak@maxlab.lu.se

ISBN 978-3-95450-134-2

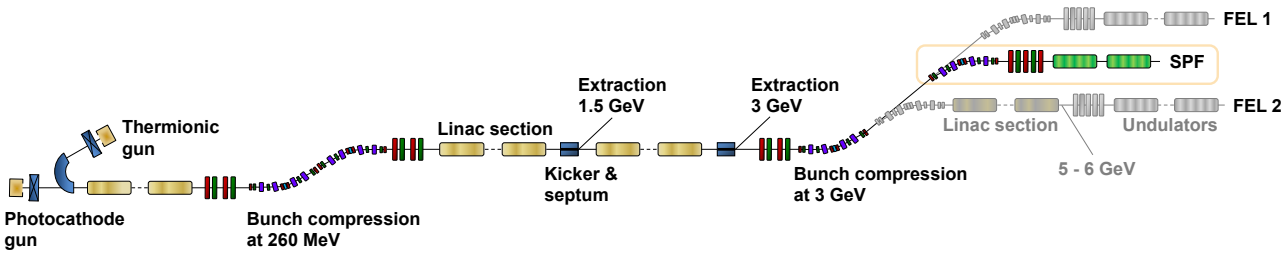

Figure 1: Schematic diagram of the SPF (in highlighted box) and its injector. Two potential FELs foreseen in the long-term strategic plan of the laboratory are shown in grey.

Table 1: Main Parameters of the Two Operation Modes Selected for the Simulation Studies

Parameter	Case A	Case B
Electron beam energy (GeV)	1.8	0.5
RMS bunch length (μm)	8	8
Peak current (kA)	2.5	2.5
Normalized emittance (μm rad)	0.4	0.4
Relative energy spread	1×10^{-4}	1×10^{-4}
Average β function (m)	13	11
Undulator period (mm)	15	15
Undulator parameter K	2.1	1.8
Radiation wavelength (nm)	2	20
Pierce parameter ρ	0.0017	0.0039
Estimated L_{sat} (m)	9	4
Estimated P_{sat} (GW)	7.7	4.8

RESULTS AND DISCUSSIONS

General Results for Case A

The results of the GENESIS time-dependent simulation for case A are summarized in Fig. 2.

Figure 2(a) shows the radiation power as a function of the distance z along the undulator line. Within the first undulator module ($z \leq 5$ m), the radiation does not exhibit any appreciable growth. Exponential growth occurs within the second undulator module ($z = 6 - 11$ m). At the exit of the undulator line ($z = 11$ m), the final power is 2.64 GW. While the estimated saturation length is $L_{\mathrm{sat}} = 9$ m, power saturation is not seen within the total undulator length of $L_w = 10$ m.

Figure 2(b) shows the evolution of the beam sizes along the undulator line. The blue and red solid curves correspond to the rms radius of the electron beam in the horizontal and vertical planes, respectively. The green dotted curve corresponds to the rms radius of the optical beam. At $z = 3 - 5$ m, the effect of optical guiding manifests itself in the decrease in optical beam size. In the break section ($z = 5 - 6$ m), the increase in optical beam size is due to vacuum diffraction. In the second undulator module ($z = 6 - 11$ m), the exponential power growth [see Fig. 2(a)] causes strong gain guiding, and hence a rapid decrease in optical beam size. At around $z = 10$ m, the decrease slows down, and the optical beam size approaches a turning point. This reflects the weakening of gain guiding, which is an indication that the radiation power is close to saturation.

Figure 2(c) shows the on-axis field amplitude as a function of z. The field grows monotonically within the undulator modules. In the break section ($z = 5 - 6$ m), there is a small decrease in field amplitude, due to the increase in the optical beam size [see Fig. 2(b)]. At around $z = 10$ m, the growth in field amplitude begins to slow down, as the power is approaching saturation.

Figure 2(d) shows the bunching factor as a function of z. Here the bunching factor is defined as the absolute value of $\langle e^{-i\psi} \rangle$, where the brackets denote the average over all particles, and ψ is the particle phase in the ponderomotive potential. The bunching factor grows with the field amplitude [see Fig. 2(c)], and the growth also begins to slow down at around $z = 10$ m. As the power is approaching saturation, the microbunching is close to fully developed, and the bunching factor reaches 0.35 at $z = 11$ m.

Sensitivity Study on Case A

The emittance, energy spread and peak current listed in Table 1 are stringent requirements on the quality of the electron beam. To quantify the effect of loosening these requirements, we perform a sensitivity study on case A using GENESIS time-dependent simulations. In particular, we probe the reduction in final radiation power (at $z = 11$ m) upon varying the emittance, the energy spread and the peak current, one at a time. The study is summarized in Table 2. The results show that the radiation power is very sensitive to the emittance and the peak current, and is fairly sensitive to the energy spread.

Single-Step Tapering in Case B

Since the SPF is made up of two variable-gap undulator modules, single-step tapering can be implemented by setting the parameters of the first and the second modules to K and $K - \Delta K$, respectively. In case B, the estimated saturation length $L_{\mathrm{sat}} = 4$ m is within the first module. By applying a single-step taper, we aim to observe post-saturation power growth in the second module.

The first module is fixed at $K = 1.8$. In GENESIS time-dependent simulations, we vary ΔK and probe the final radiation power at the exit of the second module ($z = 11$ m). The results are summarized in Fig. 3.

ISBN 978-3-95450-134-2

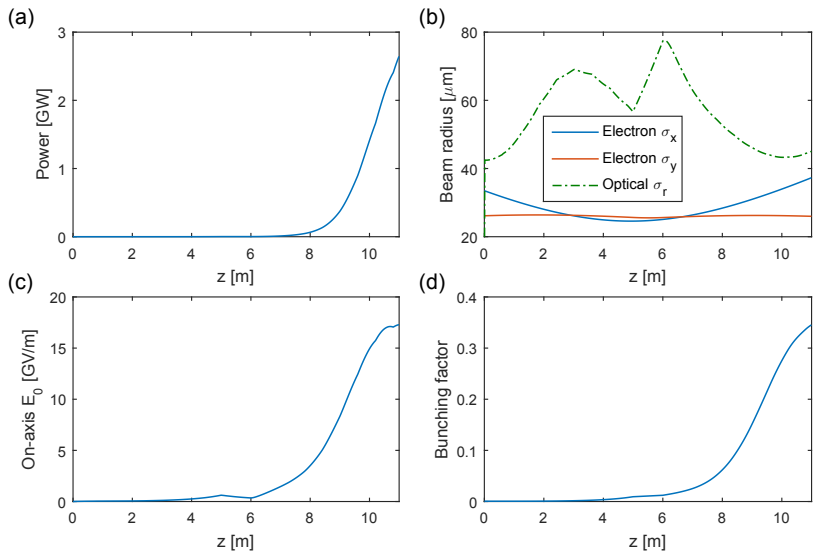

Figure 2: Simulation results for case A. The following quantities are plotted as functions of the distance z along the undulator line: (a) the radiation power; (b) the rms radii of the electron beam (solid curves) and the optical beam (dotted curve); (c) the field amplitude on axis; (d) the bunching factor.

Table 2: Results of the Sensitivity Study on Case A

Normalized emittance (μm rad)	**Final power (GW)**	**Percentage power decrease**
0.4	2.64	-
0.6	0.70	73.6%
0.8	0.13	95.0%
Relative energy spread	**Final power (GW)**	**Percentage power decrease**
1×10^{-4}	2.64	-
3×10^{-4}	1.82	31.3%
5×10^{-4}	1.06	59.9%
Peak current (kA)	**Final power (GW)**	**Percentage power decrease**
2.5	2.64	-
1.8	0.74	72.1%
1.2	0.09	96.7%

Without any tapering ($\Delta K/K = 0$), the final power is 2.58 GW. With single-step tapering, the final power is maximized at $\Delta K/K = 1.4\%$. The maximized final power is 3.51 GW, which is 36% higher than the final power in the no-taper scenario. In comparison, the theoretical estimate of the optimal $\Delta K/K$, given by Eq. (4), is 1.8%.

In Fig. 4, we compare the evolution of various quantities in the simulations of the optimized taper ($\Delta K/K = 1.4\%$) and no taper ($\Delta K/K = 0$).

As seen in Figure 4(a), the radiation power grows exponentially between $z = 3$ m and 5 m. Saturation is reached at the end of the first undulator module ($z = 5$ m), which is a little further than the estimated 4 m. The saturation power is 2.58 GW, which is lower than the estimated 4.8 GW. Without

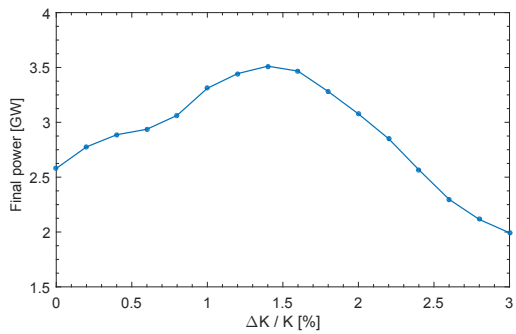

Figure 3: Simulation results for single-step tapering in case B. The final radiation power at the exit of the undulator line is plotted as a function of the step size $\Delta K/K$.

tapering, the power remains at the same level subsequently. With the optimized single-step taper, the power continues to grow after the 1-metre break section, and reaches final saturation at around $z = 7$ m in the second module.

In Figure 4(b), the decrease in optical beam size between $z = 3$ m and 5 m matches the regime of the exponential power growth, due to gain guiding. After the exponential regime, the optical beam size increases again, due to the absence of gain guiding.

In Figure 4(c), the on-axis field amplitude reaches its maximum at $z = 5$ m. Beyond the power saturation, the curve for optimized taper shows an additional bump at $z = 6 - 8$ m over the curve for no taper.

In Figure 4(d), the bunching factor also reaches its maximum at $z = 5$ m. Beyond the power saturation, the optimized taper yields a smaller bunching factor than in the case of no taper. This can be attributed to the detrapping of particles during the deceleration of the ponderomotive bucket in phase space.

ISBN 978-3-95450-134-2

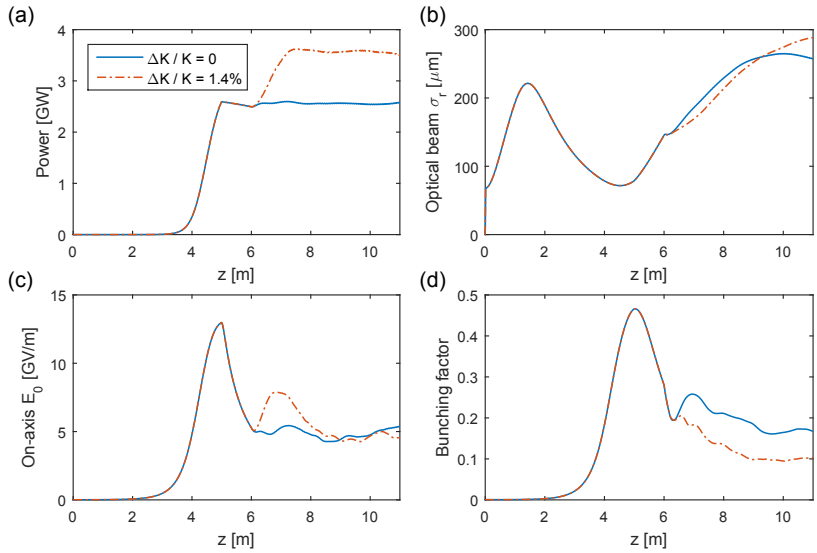

Figure 4: Simulation results for optimized taper ($\Delta K/K = 1.4\%$) and no taper ($\Delta K/K = 0$) in case B. The following quantities are plotted as functions of z: (a) the radiation power; (b) the rms radius of the optical beam; (c) the field amplitude on axis; (d) the bunching factor.

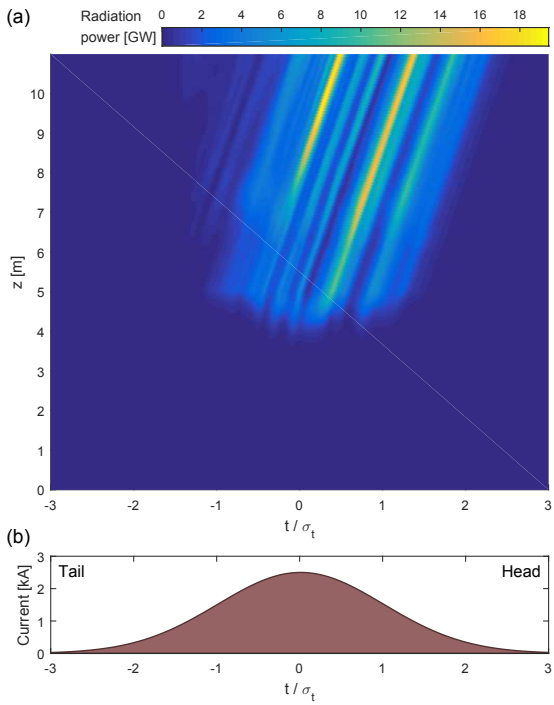

Figure 5: Simulation results for the optimized taper ($\Delta K/K = 1.4\%$) in case B. (a) Radiation power of different slices within the electron bunch. (b) The longitudinal profile of the electron bunch.

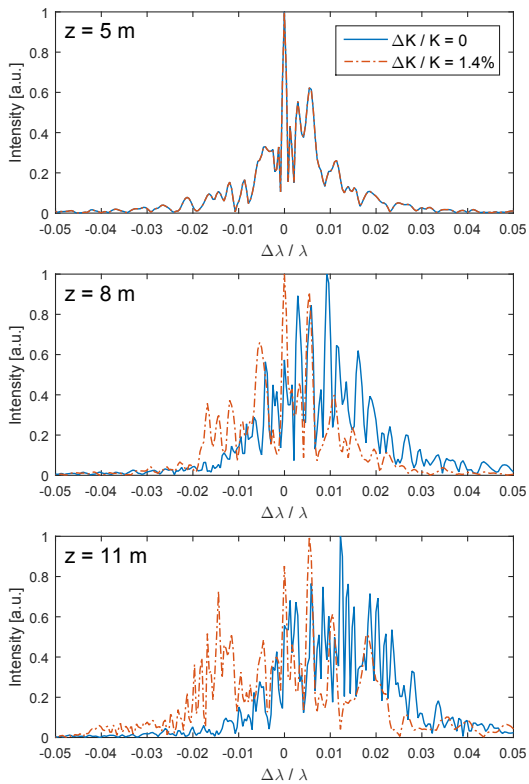

Figure 6: Spectral intensity spectra for optimized taper ($\Delta K/K = 1.4\%$) and no taper ($\Delta K/K = 0$) at $z = 5$ m, 8 m and 11 m.

Radiation Properties of Case B

As the simulations are performed in the time-dependent mode, we can also compare the radiation power at different slices within the electron bunch. This comparison is made in Fig. 5(a) for the case of optimized taper ($\Delta K/K = 1.4\%$). The colour scale shows the radiaion power. The vertical axis shows the distance z along the undulator line. The horizontal axis shows the longitudinal position t within the electron bunch, normalized to the rms bunch length σ_t. Meanwhile, the longitudinal profile of the electron bunch is shown in Fig. 5(b).

ISBN 978-3-95450-134-2

From Fig. 5(a), we see that the radiation is the most intense in the second undulator module ($z = 6-11$ m). Furthermore, it is the central part of the electron bunch ($-\sigma_t \leq t \leq 2\sigma_t$) that contributes significantly to the average radiation power shown in Figure 4(a). Towards the head and the tail of the bunch, the contribution is much smaller.

In Fig. 6, we compare the spectral intensity distributions for the scenarios of optimized taper ($\Delta K/K = 1.4\%$) and no taper ($\Delta K/K = 0$). At $z = 5$ m, the radiation power has just reached saturation, there is very little difference in the two spectral intensity distributions.

Beyond the saturation point, the single-step taper sustains the radiation at the central wavelength, and the central spike is still seen in the spectral intensity distribution at $z = 8$ m and 11 m (see Fig. 6). But in the no-taper scenario, the original resonant condition is no longer maintained after the saturation point. As a result, the radiation power shifts towards longer wavelength in the spectral intensity distributions for $z = 8$ m and 11 m (see Fig. 6).

Another observation in the spectral intensity distribution is the growth of sidebands (see Fig. 6). For the optimized taper, at $z = 11$ m, sidebands are seen around $\Delta\lambda/\lambda = 0.018$ and -0.014. The sideband at $\Delta\lambda/\lambda = 0.005$ even surpasses the central spike in intensity. The growth of the sidebands can be attributed to synchrotron oscillations [7].

CONCLUSION AND OUTLOOK

In this article, we have discussed two operation modes of the SPF, referred to as case A and case B. With the use of time-dependent simulations in GENESIS, we have demonstrated that these operation modes lead to exponential power growth within the length of the undulator line. In these operation modes, the SPF functions as a simple FEL.

In case A, we have performed a sensitivity study, quantifying the effect on the radiation power after loosening the requirements on the quality of the electron beam.

In case B, we have applied the technique of single-step tapering, and compared the optimal step size $\Delta K/K$ obtained in our simulations to that given by theoretical estimation in Li and Jia [5]. With the simulation results, we have examined the radiation properties, which include the evolution of the spectral intensity distribution along the undulator line.

Beyond this article, we envision to test the two FEL operation modes experimentally at the SPF. The experience of operating the SPF as a simple FEL shall provide insight into the laboratory's future development of a full-fledged FEL.

REFERENCES

[1] S. Werin et al., "Short Pulse Facility for MAX-lab", Nucl. Instrum. Methods Phys. Res., Sect. A **601**, 98 (2009).

[2] F. Curbis et al., "Towards an X-Ray FEL at the MAX IV Laboratory", in Proceedings of the 36th International Free-Electron Laser Conference, Basel, Switzerland, 549 (2014).

[3] S. Reiche, "GENESIS 1.3: a Fully 3D Time-Dependent FEL Simulation Code", Nucl. Instrum. Methods Phys. Res., Sect. A **429**, 243 (1999).

[4] D. A. Jaroszynski et al., "Free-Electron Laser Efficiency Enhancement, Gain Enhancement, and Spectral Control Using a Step-Tapered Undulator", Phys. Rev. Lett. **74**, 2224 (1995).

[5] H. Li, Q. Jia., "Optimization of Single-Step Tapering Amplitude and Energy Detuning for High-Gain FELs", Chinese Physics C **39**, 018101 (2015).

[6] Z. Huang, K.-J. Kim, "Review of X-Ray Free-Electron Laser Theory", Phys. Rev. ST Accel. Beams **10**, 034801 (2007).

[7] R. W. Warren, J. C. Goldstein, "The Generation and Suppression of Synchrotron Sidebands", Nucl. Instrum. Methods Phys. Res., Sect. A **272**, 155 (1988).

ISBN 978-3-95450-134-2